Science of the Total Environment 609 (2017) 621–632

Contents lists available at ScienceDirect

Science of the Total Environment

journal homepage: www.elsevier.com/locate/scitotenv

Evaluating a Bayesian modelling approach (INLA-SPDE) for environmental mapping

Jingyi Huang [a,b], Brendan P. Malone [a], Budiman Minasny [a,*], Alex B. McBratney [a], John Triantafilis [b]

[a] Sydney Institute of Agriculture & School of Life and Environmental Sciences, The University of Sydney, Eveleigh, NSW 2015, Australia
[b] School of Biological, Earth and Environmental Sciences, Faculty of Science, UNSW Sydney, Kensington, NSW 2052, Australia

HIGHLIGHTS

- INLA-SPDE used to predict skewed and non-skewed environmental variables.
- The model performance of INLA-SPDE was equivalent to REML-LMM.
- INLA-SPDE was able to estimate the pdfs of model parameters and responses.
- INLA-SPDE was as robust as REML-LMM with sparse datasets (e.g. 40–60).
- INLA-SPDE can be applied in environmental monitoring and management.

GRAPHICAL ABSTRACT

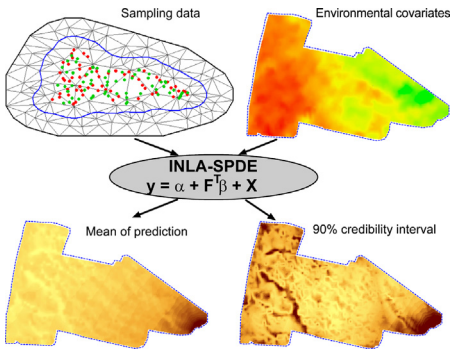

ARTICLE INFO

Article history:
Received 15 May 2017
Received in revised form 19 July 2017
Accepted 23 July 2017
Available online xxxx

Editor: Wei Ouyang

Keywords:
Elevation
Gamma-ray spectrometry
X-ray fluorescent
Sample size
Markov chain Monte Carlo
Stochastic partial differential equation

ABSTRACT

Understanding the uncertainty in spatial modelling of environmental variables is important because it provides the end-users with the reliability of the maps. Over the past decades, Bayesian statistics has been successfully used. However, the conventional simulation-based Markov Chain Monte Carlo (MCMC) approaches are often computationally intensive. In this study, the performance of a novel Bayesian inference approach called Integrated Nested Laplace Approximation with Stochastic Partial Differential Equation (INLA-SPDE) was evaluated using independent calibration and validation datasets of various skewed and non-skewed soil properties and was compared with a linear mixed model estimated by residual maximum likelihood (REML-LMM). It was found that INLA-SPDE was equivalent to REML-LMM in terms of the model performance and was similarly robust with sparse datasets (i.e. 40–60 samples). In comparison, INLA-SPDE was able to estimate the posterior marginal distributions of the model parameters without extensive simulations. It was concluded that INLA-SPDE had the potential to map the spatial distribution of environmental variables along with their posterior marginal distributions for environmental management. Some drawbacks were identified with INLA-SPDE, including artefacts of model response due to the use of triangle meshes and a longer computational time when dealing with non-Gaussian likelihood families.

1. Introduction

Understanding the uncertainty in spatial modelling is important because it provides the end-users with the reliability of the maps (McBratney, 1992; Bishop et al., 2006; Minasny and McBratney, 2016;

* Corresponding author.
E-mail address: budiman.minasny@sydney.edu.au (B. Minasny).

http://dx.doi.org/10.1016/j.scitotenv.2017.07.201
0048-9697/

Rong et al., 2017). Over the past decades, various sources of uncertainty have been identified associated with the spatial models, input data, analytical errors and instrumental noises (Heuvelink et al., 2006; Nelson et al., 2011; Chen et al., 2014). Much effort has been taken to understand and minimise the analytical errors (Viscarra Rossel and McBratney, 1998) and instrumental noises (Sudduth et al., 2001; Nelson et al., 2011; Huang et al., 2015; Huang et al., 2017a).

In terms of the uncertainty in the spatial models, Bayesian statistics has been successfully used (D'Or and Bogaert, 2003; Zhou et al., 2004; Douaik et al., 2005; Kavetski et al., 2006; Brus et al., 2008; Yang et al., 2009; Minasny et al., 2011; Liang et al., 2016). Compared with the frequentist statistics which assumes the model parameters to be deterministic, the Bayesian inference approach considers the model parameters as probabilistic variables with joint posterior probability density functions (pdfs) and can be used to incorporate external information (Gelman et al., 2004). The use of posterior pdfs also makes Bayesian statistics easier to account for the uncertainty in variance components of predictive models compared to a frequentist approach (Diggle et al., 1998).

To obtain the posterior distribution of model parameters, simulation-based approaches such as Markov Chain Monte Carlo (MCMC) simulation are common. However, this type of approach is computationally intensive (Minasny et al., 2011; Milledge et al., 2012). An alternative numerical approximation approach, called the Integrated Nested Laplace Approximation (INLA), has recently been proposed (Rue et al., 2009). Unlike MCMC, INLA allows relatively fast Bayesian inference by using numerical approximations to the marginal density for the hyper-parameters and latent variables (Ryan et al., 2016). When combined with a Stochastic Partial Differential Equation (SPDE) for modelling the spatial correlation, INLA-SPDE has shown advantages in various fields, including spatio-temporal diseases mapping (e.g., Schrödle and Held, 2011; Musenge et al., 2013) and spatial modelling of environmental variables associated with large data (e.g. Eidsvik et al., 2012; Poggio et al., 2016).

However, few researchers have evaluated the performance of INLA-SPDE using independently collected calibration and validation datasets and the performance of INLA-SPDE on the sparse environmental datasets has been little studied. To further evaluate the potential use and application of INLA-SPDE in modelling and mapping environmental variables, the aims of this study was tri-fold; 1) to map the spatial distribution of various skewed and non-skewed soil properties and elemental data and estimate their posterior marginal distributions using INLA-SPDE; 2) to compare the model performance of INLA-SPDE with a commonly used linear mixed model estimated by residual maximum likelihood (REML-LMM) using independent calibration and validation datasets that were collected by stratified random sampling; 3) to evaluate the robustness of INLA-SPDE and REML-LMM on the sparse datasets.

2. Materials and methods

2.1. Study area

The study area is located in the E. J. Holtsbaum Agricultural Research Station, also known as the Nowley farm. It covers an area of approximately 2300 ha (Fig. 1). The town Nowley is located on the North West Slopes and Plains of New South Wales, Australia. The mean annual maximum and minimum temperatures are 24.6 and 12.2 °C, respectively, and the annual precipitation is on average 636.9 mm (BOM, 2016).

On the upper slopes and at the eastern end of the property, shallow and stony soils from weathered basalt are present. These soils grade into deeper and dark-coloured Vertosols (World Reference Base equivalent Vertisols, Soil Taxonomy equivalent Udic Haplusterts) in the upper mid-slope and mid-slope positions. Also prominent in these mid-slope positions are texture-contrast Chromosols (World Reference Base equivalent Luvisols, Soil Taxonomy equivalent Udic Rhodustalfs), while in the lower slope positions poorly drained, grey-brown Vertosols (World Reference Base equivalent Vertisols, Soil Taxonomy equivalent Sodic Gypsiusterts), and texture-contrast Sodosols (World Reference Base equivalent Solonetz, Soil Taxonomy equivalent Aquic-Arenic Natrustalfs) are present (Stockmann et al., 2016). The eastern parts of the farm are dominated by native vegetation while western parts are mainly used for cropping.

2.2. Ancillary data collection

The farm was initially surveyed using an on-the-go proximal soil sensing system in 2004. Information on the locations was recorded automatically along with the elevation data using a Real-Time Kinetic Global Positioning System. The approximate spacing of the proximal survey lines was 20 m. Airborne gamma-ray radiometrics data were also obtained from the Department of Mineral Resources, New South Wales, Australia. The elevation and gamma radiometrics data were interpolated on a regular 10 m × 10 m grid using kriging with local variograms. Based on the elevation data, slope and topographic wetness index (TWI) were calculated using SAGA GIS (Conrad et al., 2015).

Soil samples were collected and analysed for soil pH and carbon content in the 2004 survey. Initial digital soil maps of total soil carbon percentage (soil C) and pH, along with their uncertainties, were generated using the regression kriging approach (De Gruijter et al., 2016). These initial maps of soil C and pH were only used for guiding the yet to be described sampling design, and should not be confused with the maps of predicted soil C and pH using INLA-SPDE or REML-LMM approach which will be discussed below.

2.3. Soil sampling and laboratory analysis

2.3.1. Soil sampling design

Independent calibration and validation datasets need to be collected. A stratified random sampling design was generated using the initial maps of carbon and pH as inputs to the Ospats algorithm (De Gruijter et al., 2015), which optimised spatial stratification. The first sampling design was based on the initial map of pH and was called dataset A. The second sampling design was based on the initial map of carbon, and was called dataset B. The sampling campaign was conducted in February 2014, with 60 sites in each data set located using a handheld GPS and samples were collected from the top 7.5 cm. In addition, at each of the pre-determined sites, an extra sample was located 1 m from the predetermined location in a random orientation to account for the short-range variability. Thus the total number of samples is 120 in both dataset A & B.

Fig. 2a shows the location of the 120 sample site locations which were used for calibration (dataset A) and the 120 samples that were available for validation (dataset B). These calibration and validation datasets were used for evaluating the SPDE-INLA and REML-LMM models for predicting total soil Fe, Ca, K, Ti/Zr ratio and pH.

2.3.2. Laboratory analysis

All samples were taken back to the laboratory, air-dried, crushed, and passed through a 2-mm sieve. Soil pH (1:5 soil to water) was measured. Soil C were analysed using the dry combustion method with the CNS analyser (Vario Max Analyser, Hanau, Germany). A portable XRF was used to measure the elemental concentration of the soil samples. The portable X-ray Fluorescence spectrometer (pXRF) (Olympus Delta TA Premium pXRF analyses; Olympus, Centre Valley, PA, USA) was used to measure total concentrations of ~40 elements in the soil samples. Each sample was scanned under three beams (50 kV, 40 kV, and 15 kV) with five replicates, and its average value was used as the measure of total elemental concentrations.

Prior to taking pXRF measurements, the instrument was calibrated using an Alloy 316 stainless steel calibration check standardization coupon, containing 16.13% Cr, 1.78% Mn, 68.76% Fe, 10.42% Ni, 0.20% Cu and 2.10% Mo, and the scanning of a Si blank to detect potential

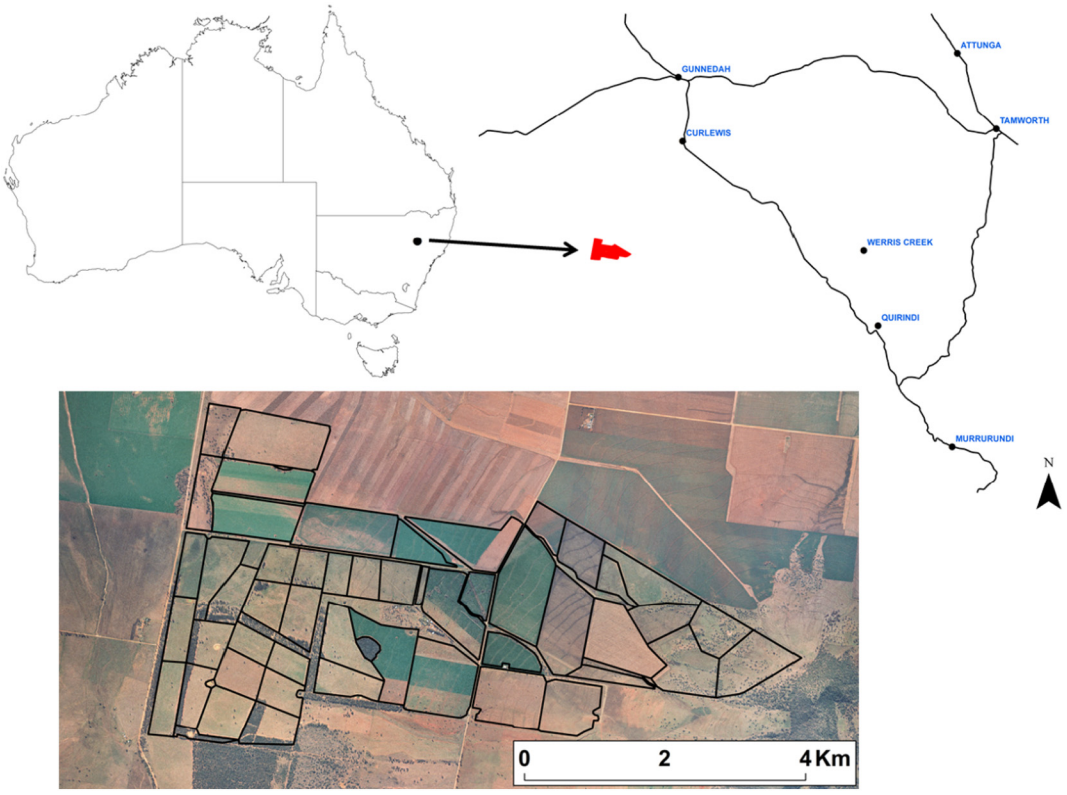

Fig. 1. Location of Nowley with reference to the position within Australia and proximity to Gunnedah, NSW, the nearest regional centre. Note: Field boundaries were overlaid upon the aerial photo of Nowley.

contamination on the pXRF measurement window. The performance of the pXRF instrument was verified using a range of NIST soil standards with varying elemental concentrations (SRM 2709, SRM 2710, and SRM 2711a). Performance results of NIST SRM 2709, San Joaquin soil, for the elements of interest in this study were (pXRF reported/NIST certified [recovery]): K, 20,300/18,854 mg kg^{-1} [1.08]; Ca, 18,900/19,581 mg kg^{-1} [0.97], Mn 538/527 mg kg^{-1} [1.02]; Ti, 3420/3341 mg kg^{-1} [1.02]; Zr, 160/123 mg kg^{-1} [1.30]; Si, 29.66/27.84% [1.07]; Al, 7.5/6.56% [1.14]; Fe, 3.5/3.84% [0.91].

2.3.3. Selecting the environmental variables and covariates

For the purposes of this study, several key soil elements were investigated, including K (%), Ca (%), and Fe (%). In addition, Ti and Zr were studied which characterise the immobile elements. The Ti/Zr ratio was used because this ratio may indicate the source and nature of parent material (Stockmann et al., 2016). With regard to soil pH and elemental concentrations (i.e., K, Ca, Fe and Ti/Zr ratio), dataset A (120 samples) were used to calibrate the spatial models (shown as solid circles in Fig. 2a), and dataset B (120 samples) used for validation (shown as hollow circles in Fig. 2a).

Soil C was also selected as it indicated soil fertility and land suitability (Li et al., 2015a; Huang et al., 2017b). In terms of predicting soil C, due to budget constraints, only 80 samples from dataset B were analysed for soil C content. These 80 samples were used to calibrate the spatial model (shown as solid circles in Fig. 2b). For validation, another 51 samples from an independent design-based sampling conducted in 2015 (De Gruijter et al., 2016) were included and analysed for carbon content (shown as hollow circles in Fig. 2b). It was called dataset C and it was only used as a validation set for soil C.

For the sake of brevity, only elevation, slope, TWI and Gamma potassium of the gamma radiometrics data (Gamma-K) were considered as cov0ariates for predicting various soil properties using INLA-SPDE and REML-LMM.

2.4. INLA-SPDE

Consider a random field **X** with realisations at locations $s_1, s_2, \ldots, s_n$: $X(s_1), X(s_2), \ldots, X(s_n)$ which are normally distributed with 0 mean and joint covariance which can be represented as a Matérn covariance function:

$$Cov(X(s_i), X(s_j)) = \sigma_e^2 \delta_{ij} + \frac{\sigma_x^2}{2^{\nu-1}\Gamma(\nu)} (\kappa||s_i - s_j||)^{\nu} K_{\nu}(\kappa||s_i - s_j||) \quad (1)$$

where $||s_i - s_j||$ is the Euclidean distance between two points s_i and s_j, σ_x^2 is the variance, κ is a scale parameter, ν is a smoothness parameter, K_ν is the modified Bessel function of the second kind, and Γ is the Gamma function (Minasny and McBratney, 2005). The Matérn function also has a noise variance σ_e^2 (i.e. the nugget effect) and δ_{ij} is the Kronecker delta: $\delta_{ij} = 0$ when $i = j$; $\delta_{ij} = 1$ when $i \neq j$.

The SPDE is based on the representation of the Matérn covariance function as a solution to the following function (Lindgren et al., 2011):

$$(\kappa^2 - \Delta)^{\omega/2} \mathbf{X}(s) = \mathbf{W}(s), s \in \mathbb{R}^2, \quad (2)$$

where $\mathbf{X}(s)$ is the random environmental variable at location s, $\mathbf{W}(s)$ is white noise, Δ is the Laplace operator $\partial^2/\partial s_1^2 + \partial^2/\partial s_2^2$ (s_1 and s_2 represent the coordinates in the two-dimensional space), ω is a positive integer related to the smoothness parameter ν and $\omega = \nu + 1$ (Lindgren and Rue, 2015). In this study $\nu = 0.5$. This made the Matérn function become an exponential covariance function and ω value became 1.5. Further, the SPDE makes an approximation of the continuous variable $\mathbf{X}(s)$ as piecewise linear functions and this produces substantial computational advantages (Blangiardo et al., 2013). Detailed descriptions about the basis functions and the approximation process can be found in Simpson et al. (2012) and Blangiardo et al. (2013).

The objectives of the Bayesian computation are the marginal posterior distributions for each of the elements of the parameters vector and

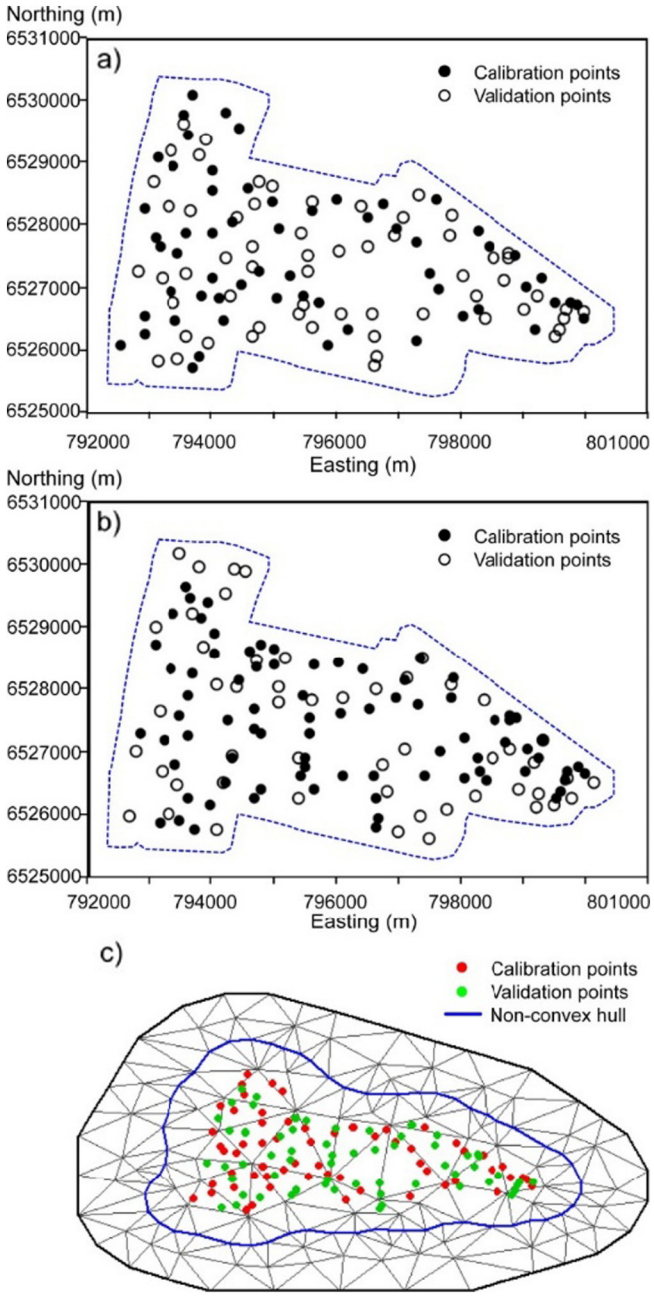

Fig. 2. a) Locations of soil sampling sites for a) total soil Fe, Ca, K, Ti/Zr ratio, pH and b) total soil carbon (C) across the study area; c) the mesh constructed using the calibration points shown in Fig. 2a. Note: Calibration and validation points were marked in solid and hollow circles in Fig. 2b and c and in red and green circles in Fig. 2d, respectively.

for each element of the hyper-parameters vector. These marginal posterior distributions were estimated based on Bayes' theorem using integrated nested Laplace approximation (INLA) method introduced by Rue et al. (2009). The INLA approach exploits the assumptions of the model to produce a numerical approximation to the posteriors of interested parameters, based on the Laplace approximation (Tierney and Kadane, 1986). Details about the theory and implementation of INLA-SPDE can be found in Rue et al. (2009), Martins et al. (2012), Blangiardo et al. (2013) and Krainski et al. (2016). INLA-SPDE was carried out using the R Package R-INLA (http://www.r-inla.org/) implemented in the R software (R Core Team, 2017).

Here, the steps of INLA-SPDE were described as follows.

1) Construct non-convex hull meshes. Because the spatial correlation structure for the SPDE part of the model was defined by the meshes and evaluated at the mesh discretisation points (Lindgren and Rue, 2015), meshes were needed for the calibration and validation datasets and for the whole prediction grid (10 m spacing). Herein, the Constrained Refined Delaunay Triangulation was used with the "inla.mesh.2d" function. The maximum triangle edge lengths were set to be 4 km in the inner domain and in the outer extension. These values were empirically determined so triangles were as regular as possible in size and shape (Krainski et al., 2016). Additionally, a minimum distance between points was empirically set to be 300 m to avoid small triangles as suggested by Krainski et al. (2016).

Although increasing the number of triangles in the mesh will slightly increase the model performance, it did not generate better modelling results based on our leave-one-out cross-validation results. Therefore, a denser mesh suggested by Poggio et al. (2016) was not used. The mesh constructed using dataset A and the corresponding 60 extra samples was shown in Fig. 2c.

2) Calculate a projection matrix. Because the SPDE model was defined on the mesh, the process at the mesh vertices required to be projected to the locations response. Details about the calculation of the projector matrix can be found in Lindgren (2012).
3) Define an SPDE model based on the mesh of the calibration dataset. Here the Matérn correlation function was used which was available in R-INLA (see Eq. 1).
4) Construct a hierarchical model. According to Krainski et al. (2016), the hierarchical model implemented in INLA-SPDE includes three effects (i.e. intercept, the fixed effect, and random effect) and can be expressed as follows:

$$\mathbf{y} = \alpha + \boldsymbol{F}^T\boldsymbol{\beta} + \mathbf{X}, \tag{3}$$

where $\mathbf{y}$ is the model response (e.g. soil pH), α is the intercept, $\mathbf{F}$ is a matrix of fixed effects or covariates (e.g., elevation, slope, TWI and Gamma-K) with coefficients $\boldsymbol{\beta}$. As defined in Eq. 1, $\mathbf{X}$ is the latent Gaussian field, used to model the random effect. The hyperparameters $\theta = (\theta_1,\theta_2)$, control the latent Gaussian field and/or the likelihood of the variables (Rue et al., 2016). θ_1 is the logarithm of the 'local variance parameter' τ such that the variance $\sigma_x^2 = \frac{1}{4\pi\tau^2\kappa^2}$; $\theta_2 = \log(\kappa)$.For reference of the various latent models used to model the latent Gaussian field ($\mathbf{X}$), readers can refer to the following link (http://www.r-inla.org/models/latent-models).

5) Fit the hierarchical model. The likelihood family of the probability distribution of the model response needed to be defined. Herein, two likelihood families (i.e. Gaussian and log-normal) were compared for all soil properties because they accounted for the distributions of most of the soil properties. In the current version of INLA-SPDE, the log-normal family simply implements log-transformation of the model response (i.e. soil properties) for the modelling process (http://www.math.ntnu.no/inla/r-inla.org/doc/likelihood/lognormal.pdf).
6) Select the optimal linear covariates. To determine the optimal combination of covariates for the fixed effects, a full INLA model was firstly fitted with all covariates (i.e., elevation, slope, TWI, and Gamma-K). Then each of the covariates was dropped in turn. Following Rue et al. (2009), the deviance information criterion (DIC) of the full model and the reduced models was calculated. A covariate was dropped if the reduced model excluding this covariate had a smaller DIC value than the full model and other reduced models. Subsequently, each of the remaining covariates was dropped in turn. Then the DIC values were calculated and another covariate was dropped based on the same criteria. The process continued until

Table 1
Summary statistics of measured soil properties for calibration and validation sets.

	Dataset	N	Min	Mean	Median	Max	SD	Skewness	CV (%)
Calibration									
K (%)	A	120	0.2	0.5	0.4	2.5	0.3	3.2	60.0
Ca (%)	A	120	0.0	0.5	0.2	2.2	0.5	1.4	114.8
Fe (%)	A	120	0.4	3.7	2.8	9.9	2.7	0.7	72.9
Ti/Zr	A	120	0.001	0.002	0.002	0.006	0.001	1.5	43.6
pH	A	120	4.9	6.4	6.3	8.3	0.8	0.4	13.1
C (%)	B	80	0.7	1.8	1.4	9.2	1.3	3.5	68.8
Validation									
K (%)	B	120	0.2	0.6	0.5	1.4	0.3	1.0	49.7
Ca (%)	B	118	0.0	0.6	0.2	2.9	0.7	1.6	115.9
Fe (%)	B	120	0.4	4.1	3.7	10.2	2.8	0.6	67.6
Ti/Zr	B	120	0.001	0.002	0.002	0.006	0.001	1.5	48.4
pH	B	120	5.1	6.5	6.5	8.4	0.8	0.3	12.5
C (%)	C	51	0.5	1.7	1.5	7.8	1.1	3.4	65.8

dropping any of the remaining covariates generated models that had larger DIC values than those of other models calculated in the same turn.

7) Estimate the posterior distribution of the parameters of the selected models. Here, the marginal distribution of the intercept, fixed effect parameters β, and parameters of the Matérn function $(\sigma_x^2, \kappa, \sigma_\varepsilon^2)$ was estimated using INLA-SPDE.
8) Predict the soil properties onto the validation datasets.

Here, a number of metrics between the measured and predicted soil properties were employed using the validation datasets to evaluate the model performance. These include coefficient of determination (R^2), Lin's concordance correlation coefficient (Lin, 1989), mean error (ME) and root mean square error (RMSE).

9) Predict the soil properties and calculate their posterior marginal distribution across the whole study area.

2.5. REML-LMM

The linear mixed model (LMM) includes a fixed effect component, which is a relationship between the response (e.g. soil C) and the ancillary data (e.g. elevation), a spatial correlation model (i.e. variogram) to model spatial dependence, the random effect, and an error component ($\boldsymbol{\varepsilon}$). A LMM often has the form:

$$\mathbf{y} = \mathbf{B}\boldsymbol{\tau} + \mathbf{u} + \boldsymbol{\varepsilon}, \tag{4}$$

where $\mathbf{y}$ is a vector of the model response, $\mathbf{B}$ is a matrix of predicting covariates (e.g. elevation) at observation points, and the vector $\boldsymbol{\tau}$ contains coefficients of the fixed effects. The vectors $\mathbf{u}$ and $\boldsymbol{\varepsilon}$ contain random errors which are spatially correlated such that

$$\begin{bmatrix} \boldsymbol{u} \\ \boldsymbol{\varepsilon} \end{bmatrix} \sim N\left(\begin{bmatrix} 0 \\ 0 \end{bmatrix}, \begin{bmatrix} \xi\sigma^2\boldsymbol{G} & 0 \\ 0 & \sigma^2\boldsymbol{I} \end{bmatrix} \right), \tag{5}$$

where $\mathbf{G}$ is the correlation matrix where correlation depends only on the relative location of observations. $\mathbf{I}$ is the identity matrix and σ^2 is the variance of the independent error and ξ is the ratio of the variance of $\mathbf{u}$ to σ^2 (Lark et al., 2006). Here it is assumed that the random terms are jointly Gaussian distributed. The term $\boldsymbol{\varepsilon}$ represents both independent measurement errors and variation of the processes that are spatially dependent over shorter distances than separate samples, namely, the nugget (σ_ε^2).

Once the parameters of the LMMs were determined, soil properties were predicted onto the unsampled locations using the formulation of universal kriging with external drift. The process is considered as the empirical best linear unbiased prediction (E-BLUP). Full details of E-BLUP can be found in Lark and Cullis (2004) and Lark et al. (2006). The geoR package (Ribeiro and Diggle, 2001) in R was used to fit the model parameters in Eqs. (4) and (5) while the gstat package (Pebesma, 2004) was used for kriging. To be consistent, the same sets of covariates selected in the INLA-SPDE models were used to construct the corresponding LMMs. Only the nugget and exponential variograms were compared and the optimal variograms were selected based on the log-likelihood. Similarly, the LMMs were fitted using the calibration datasets and various soil properties were predicted onto the validation datasets to evaluate the model performance. To validate the REML-LMM models, R^2, Lin's concordance, ME, and RMSE were also calculated.

2.6. Evaluating the effects of sampling size on the INLA-SPDE and REML-LMM

To evaluate the effects of sampling sizes on the model performance, a certain number of points were randomly selected from the calibration data (i.e. 100, 80, 60 and 40 samples for Fe, Ca, K, Ti/Zr ratio and pH and 70, 60, 50 and 40 samples for C). INLA-SPDE and REML-LMM models were constructed using these subsets of the calibration datasets and predicted onto the validation datasets.

3. Results and discussion

3.1. Exploratory data analysis

The summary statistics of various soil properties are shown in Table 1. Of all the soil properties, soil C was strongly skewed for both calibration and validation datasets (skewness = 3.5 and 3.4, respectively). Total soil Ca concentration and Ti/Zr ratio were moderately skewed (skewness ≈ 1.5) while total Fe concentration and pH were non-skewed (skewness < 1). It was also noted that soil Ca was most variable in the field (CV > 100%) while pH was least variable (CV < 20%). The remaining soil properties showed moderate variability.

The Pearson's correlation coefficients between soil properties and covariates are shown in Table 2. With regard to the calibration data, the elements that were significantly correlated with gamma-K ($P < 0.001$) included soil K ($r = 0.89$) and Fe (0.87). Whilst strong correlations have previously been reported between gamma-K and soil K (i.e. Wong and Harper, 1999; Haskard et al., 2010), the high correlation observed in this study is not very common. Gamma-K was also significantly correlated with Ti/Zr ($r = 0.67$) and Ca ($r = 0.66$). In addition, and whilst soil pH ($r = 0.63$) and soil C ($r = 0.53$) were only moderately correlated with gamma-K, they were statistically significant and these results were consistent with the findings by Wong et al. (2008) and Dierke and Werban (2013), respectively. Therefore, it was reasonable to argue that the strong correlations between soil elements and gamma-ray elements may be site-specific and were controlled by the

Table 2
Pearson's correlation coefficient (r) between various soil properties and ancillary data for the calibration and validation datasets. Note: *, <0.05; **, <0.01, ***, <0.001.

	Num.	Gamma-K	Elevation	Slope	Topographic wetness index
Calibration					
K	120	0.89***	0.59***	0.39***	−0.39***
Ca	120	0.66***	0.78***	0.63***	−0.54***
Fe	120	0.87***	0.84***	0.68***	−0.55***
Ti/Zr	120	0.66***	0.78***	0.67***	−0.50***
pH	120	0.63***	0.53***	0.37***	−0.40***
C	80	0.53***	0.53***	0.56***	−0.48***
Validation					
K	120	0.89***	0.58***	0.33***	−0.51***
Ca	118	0.78***	0.78***	0.65***	−0.52***
Fe	120	0.92***	0.81***	0.65***	−0.59***
Ti/Zr	120	0.82***	0.74***	0.60***	−0.58***
pH	120	0.57***	0.43***	0.34***	−0.28***
C	51	0.78***	0.66***	0.51***	−0.51***

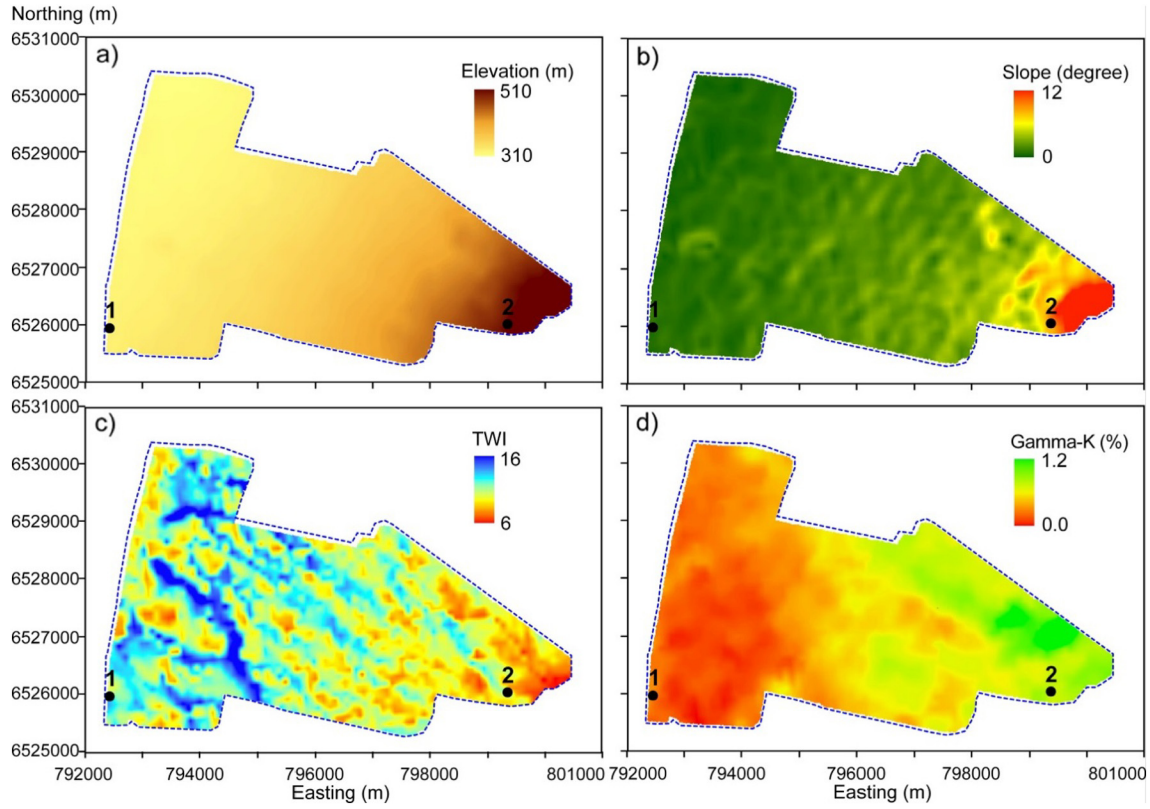

Fig. 3. Spatial distribution of the various kriged ancillary data and including; a) elevation (m), b) slope (degree), c) topographic wetness index (TWI) and d) gamma potassium (Gamma-K – %) across the study area, respectively. Note: two selected sites with predicted small and large soil properties were marked with black dots.

localised soil mineralogy composition and as a function of different physical, chemical and biological weathering processes (Triantafilis et al., 2013).

In terms of the terrain parameters, elevation was positively correlated with soil elemental data and in particular Fe ($r = 0.84$), Ti/Zr ratio (0.78), Ca (0.78) and K (0.59), as well as pH (0.53) and soil C (0.53) while topographic wetness index (TWI) was negatively correlated in comparison. Similar positive correlations were evident with slope. It was also noted that similar strong correlations were also evident in the validation data.

Table 3
Summary statistics of the model parameters of the a) INLA-SPDE and b) REML-LMM models.

a)	Mean	2.5% percentile	Median	97.5% percentile	Mode	SD
Intercept	−3.074	−4.600	−3.062	−1.619	−3.038	0.753
Gamma-K	1.303	1.011	1.304	1.588	1.307	0.146
Elevation	0.00483	0.00058	0.00480	0.00929	0.00473	0.00220
Slope	−0.055	−0.099	−0.054	−0.012	−0.054	0.022
TWI	0.023	−0.002	0.023	0.049	0.023	0.013
Variogram	Exponential function					
Scale parameter (κ)	0.00295	0.0007	0.0023	0.0089	0.0015	0.00217
σ_x^2	0.105	0.020	0.078	0.346	0.046	0.088
Practical range (m)	1021.8	222.3	852.1	2804.0	566.3	678.5
θ_1	3.363	1.999	3.384	4.621	3.438	0.666
θ_2	−6.037	−7.273	−6.057	−4.699	−6.110	0.650
Nugget (σ_e^2)	0.029	0.022	0.029	0.038	0.028	0.004
DIC	−248.399					

b)			
Fixed effects	Estimates	Standard Error	Prob > |t|
Intercept	−1.335	0.973	0.173
Gamma-K	1.521	0.156	<0.0001
Elevation	0.00355	0.00276	0.201
Slope	−0.056	0.019	0.004
TWI	0.016	0.012	0.187
Variogram	Exponential function		
partial sill	0.074		
Practical Range (m)	5991.5		
Nugget (σ_e^2)	0.004		
Scale parameter (κ)	0.0005		
Log-likelihood	91.2		

Table 4
Comparison of model statistics between INLA-SPDE and REML-LMM on the validation dataset. Note: The selected INLA-SPDE models were marked in bold.

INLA-SPDE	R^2	Lin's concordance	ME	RMSE
K (Gaussian-Mean)	0.80	0.88	−0.04%	0.14%
Ca (Gaussian-Mean)	**0.68**	**0.78**	**0.05%**	**0.38%**
Fe (Gaussian-Mean)	0.90	0.95	−0.08%	0.88%
C (Gaussian-Mean)	**0.45**	**0.65**	**−0.19%**	**0.86%**
pH (Gaussian-Mean)	**0.59**	**0.76**	**0.03**	**0.53**
Ti/Zr (Gaussian-Mean)	0.63	0.72	0.0001	0.0007
K (lognormal-Mean)	**0.83**	**0.91**	**−0.02%**	**0.12%**
Ca (lognormal-Mean)	0.65	0.75	0.11%	0.41%
Fe (lognormal-Mean)	**0.91**	**0.95**	**0.01%**	**0.85%**
C (lognormal-Mean)	0.41	0.61	−0.08%	0.86%
pH (lognormal-Mean)	0.59	0.75	0.05	0.53
Ti/Zr (lognormal-Mean)	**0.64**	**0.70**	**0.0001**	**0.0007**
K (lognormal-Median)	0.83	0.91	−0.02%	0.12%
Ca (lognormal-Median)	0.65	0.75	0.11%	0.41%
Fe (lognormal-Median)	0.91	0.95	0.01%	0.85%
C (lognormal-Median)	0.41	0.61	−0.08%	0.86%
pH (lognormal-Median)	0.59	0.75	0.05	0.53
Ti/Zr (lognormal-Median)	0.64	0.70	0.0001	0.0007
REML-LMM	R^2	Lin's concordance	ME	RMSE
K (Gaussian-Mean)	0.82	0.90	−0.03%	0.13%
Ca (Gaussian-Mean)	0.66	0.79	0.04%	0.39%
Fe (Gaussian-Mean)	0.91	0.95	−0.14%	0.82%
C (Gaussian-Mean)	0.44	0.64	−0.20%	0.87%
pH (Gaussian-Mean)	0.65	0.78	0.05	0.49
Ti/Zr (Gaussian-Mean)	0.70	0.78	0.0000	0.0006

3.2. Spatial distribution of covariates

The spatial distributions of the various covariates are shown in Fig. 3. Fig. 3a shows that the elevation was highest in the east (510 m) and decreased to topographic low in the west (310 m). Fig. 3b, which shows the slope, for the most part the study area had only a small fall (slope = 0–5 degrees) (Fig. 3b). However, to the eastern margin, elevation increased rapidly over a short distance with slope larger than 10 degrees (Fig. 3b). Fig. 3c shows the spatial distribution of TWI. It was evident that several contiguous regions of larger TWI values (i.e. 10–16) traverse the study area from southeast to the northwest. These regions were more or less consistent with the location of various depressions and the location of local small drainage ways and floodways (Fig. 1). In the west they were wooded and in the east they were protected by perennial grasses.

Fig. 3d shows the spatial distribution of gamma-K. Note that an increasing trend was found in gamma-K from southwest to the northeast of the study area. Given previous studies which have shown that gamma-K is correlated with soil parent materials (Wilford et al., 1997; Triantafilis et al., 2013), soil texture (Viscarra Rossel et al., 2007) and soil types (Schuler et al., 2011; Guimaraes et al., 2013), the differences in gamma-K was due to varying parent materials and soil types.

3.3. Comparison of the model parameters between INLA-SPDE and REML-LMM

To better understand the modelling process and compare INLA-SPDE and REML-LMM, the marginal distributions of the parameters of the INLA-SPDE model were presented. For brevity, only the scenario for predicting elemental K concentration that was moderately skewed was shown in Table 3.

In this case, after dropping each of the ancillary data in turn (Step-6 of the INLA-SPDE model calibration), it was found the DIC values increased. This indicated that all the ancillary data were required and therefore the model needed to include gamma-K, elevation, slope, and TWI as covariates.

The marginal distributions of the intercept, fixed effects parameters, scale parameter (κ) of the Matérn function, variance parameter of the random field (σ_x^2) and the practical range are shown in Table 3a. Table 3a also shows in the mean of coefficients of the fixed effects, practical range (1021.8 m), scale parameter (0.003) and nugget (0.029) of the Matérn function (with $\upsilon = 0.5$, or the exponential function) of the INLA-SPDE. The equivalent data for REML-LMM model are shown in Table 3b, including the coefficients of the fixed effects, practical range (5991.5 m), scale parameter (0.0005) and nugget (0.004) of the exponential function. The difference between the two approaches was that INLA-SPDE provides an estimate of the posterior marginal distribution (e.g. upper and lower 2.5% percentiles) of the model parameters while the traditional REML approach estimated the optimal parameter values only.

Table 5
Comparison of model statistics between INLA-SPDE and REML-LMM when different sampling sizes were used.

Soil property	Skewness	Size of calibration set	INLA-SPDE				REML-LMM			
			R^2	Lin's	ME	RMSE	R^2	Lin's	ME	RMSE
C	3.5	80	0.45	0.65	−0.19%	0.86%	0.44	0.64	−0.20%	0.87%
C	3.3	70	0.45	0.64	−0.27%	0.90%	0.44	0.64	−0.27%	0.91%
C	3.7	60	0.45	0.64	−0.23%	0.87%	0.44	0.64	−0.23%	0.88%
C	3.7	50	0.45	0.64	−0.23%	0.87%	0.44	0.64	−0.23%	0.88%
C	3.5	40	0.45	0.65	−0.31%	0.95%	0.44	0.64	−0.31%	0.96%
C	3.2	30	0.45	0.64	−0.34%	0.97%	0.44	0.64	−0.34%	0.98%
C	3.8	20	0.46	0.38	−1.31%	2.65%	0.43	0.42	−1.13%	2.22%
Ti/Zr	1.5	120	0.64	0.70	0.0001	0.0007	0.70	0.78	0.0000	0.0006
Ti/Zr	1.3	100	0.60	0.68	0.0001	0.0007	0.69	0.77	0.0001	0.0006
Ti/Zr	1.3	80	0.60	0.66	0.0002	0.0007	0.69	0.76	0.0001	0.0006
Ti/Zr	1.3	60	0.54	0.65	0.0001	0.0008	0.63	0.72	0.0001	0.0007
Ti/Zr	1.5	40	0.24	0.39	−0.0003	0.0019	0.30	0.54	−0.0000	0.0011
Ti/Zr	1.6	30	0.13	0.24	0.0004	0.0011	0.11	0.22	0.0004	0.0011
Ti/Zr	1.1	20	0.15	0.26	0.0003	0.0011	0.20	0.29	0.0003	0.0010
pH	0.4	120	0.59	0.76	0.03	0.53	0.66	0.79	0.06	0.48
pH	0.4	100	0.59	0.76	0.05	0.53	0.65	0.78	0.06	0.49
pH	0.4	80	0.62	0.77	0.04	0.51	0.65	0.78	0.03	0.49
pH	0.4	60	0.63	0.78	0.02	0.50	0.63	0.78	0.04	0.50
pH	0.6	40	0.62	0.78	0.04	0.51	0.62	0.77	0.02	0.50
pH	0.8	30	0.51	0.71	0.01	0.62	0.54	0.73	0.01	0.59
pH	1.1	20	0.21	0.39	0.37	0.85	0.58	0.68	0.22	0.57

3.4. Comparison of the model performance between INLA-SPDE and REML-LMM

Table 4 shows the validation results for predicting different soil properties using INLA-SPDE and REML-LMM. When INLA-SPDE was used, the mean of the predicted soil properties estimated using a Gaussian likelihood was reported and both the mean and median values of the soil properties estimated using a log-normal likelihood were reported. Table 4 indicates that the use of the median values for log-normal likelihood did not improve the model performance in terms of the goodness of fit (R^2 and Lin's concordance), bias (ME) and accuracy (RMSE) as compared with the mean. Therefore, the paper only focused on the mean values obtained by either Gaussian or log-normal likelihood using the INLA-SPDE approach.

With respect to the strongly skewed soil C, INLA-SPDE produced similar predictions given the RMSE (0.86%) and ME (−0.19%) were slightly smaller than REML-LMM which produced larger RMSE (0.87%) and ME (−0.20%). The Lin's concordance correlation coefficient was also slightly larger for INLA-SPDE (0.65) compared with REML-LMM (0.64).

Table 4 also shows that the INLA-SPDE was equivalent to REML-LMM for predicting the moderately skewed (i.e., elemental K, Ca and Ti/Zr) and non-skewed data (elemental Fe and pH). This was most likely due to the strong linear relationships between the soil properties and the covariates (see Table 2), which were equivalently modelled by REML-LMM and INLA-SPDE.

3.5. Effects of sampling size on the model performance

Table 5 shows the effects of sampling size on INLA-SPDE and REML-LMM approaches. For brevity, only soil C (strongly skewed), Ti/Zr ratio (moderately skewed) and pH (non-skewed) were shown as they were representative of the other results. In terms of predicting soil C, as indicated by the RMSE, the INLA-SPDE (e.g. 70 sites: 0.90%) approach achieved similar results compared with REML-LMM (e.g. 70 sites: 0.91%) when sampling size decreased from 80 to 30. This suggests that INLA-SPDE was equivalent to LMM-REML for predicting strongly skewed soil properties even when sample size was small.

However, this was not the case for Ti/Zr ratio. As the sample size decreased from 120 to 60, REML-LMM (e.g. 100 sites: RMSE = 0.0006) generally performed better than or equivalent to INLA-SPDE (e.g. 100 sites: RMSE = 0.0007). When the sample size was <60, both predictions became very poor (Lin's concordance < 0.6). These results indicated that INLA-SPDE was slightly less robust than REML-LMM for predicting moderately skewed soil properties. With regard to the non-skewed soil pH, both INLA-SPDE and LMM-REML achieved good results even when the sampling size decreased to 40 (Lin's concordance >0.6).

It was not expected that LMM-REML was robust for predicting soil properties with a small number of samples (Lark et al., 2006; Minasny and McBratney, 2007; Minasny et al., 2008; Li et al., 2015b). However, the results of this study showed that INLA-SPDE was able to achieve equivalent model performance with sparse calibration data.

3.6. Posterior distribution of predicted soil properties using INLA-SPDE

To evaluate the model performance for predicting different soil properties, the posterior distribution of the predicted soil properties was plotted using two selected sites with small and large values (marked in Figs. 3, 5 and 6). Fig. 4a shows the posterior distribution of predicted strongly skewed soil C at sites 1 and 2. The distributions were close to normal due to the use of the Gaussian function for INLA-SPDE model. Additionally, higher C value at site 2 had a smaller kurtosis compared with the lower C value at site 1.

The larger uncertainty in prediction at site 2 was most likely a function of the highly variable spatial nature of the ancillary data used to develop the INLA-SPDE; namely elevation and TWI. This was most apparent with respect to the TWI data shown in Fig. 3c. Site 2 was located in a local topographic low (i.e. TWI ~12). However, it was surrounded on all three sides by topographic highs (TWI ~6–8). As a result, this caused a wider spread in the posterior distribution.

Similar patterns were identified for the posterior marginal distributions of moderately skewed Ti/Zr ratio (Fig. 4b) and pH (Fig. 4c). Again, the distributions of the model response (Ti/Zr ratio and pH) were flatter (small kurtosis) at site 2 compared with site 1. With respect to the Ti/Zr ratio, prediction required elevation and slope be used as the covariates in the INLA-SPDE approach. However, there was marked spatial variability around site 2. This was especially the case with respect to the slope (see Fig. 3b) which was steeper to the east (~12 degrees) than to the west (~6–8 degrees). The same applied for pH; whereby elevation and TWI were the ancillary data and for the same reason as soil C.

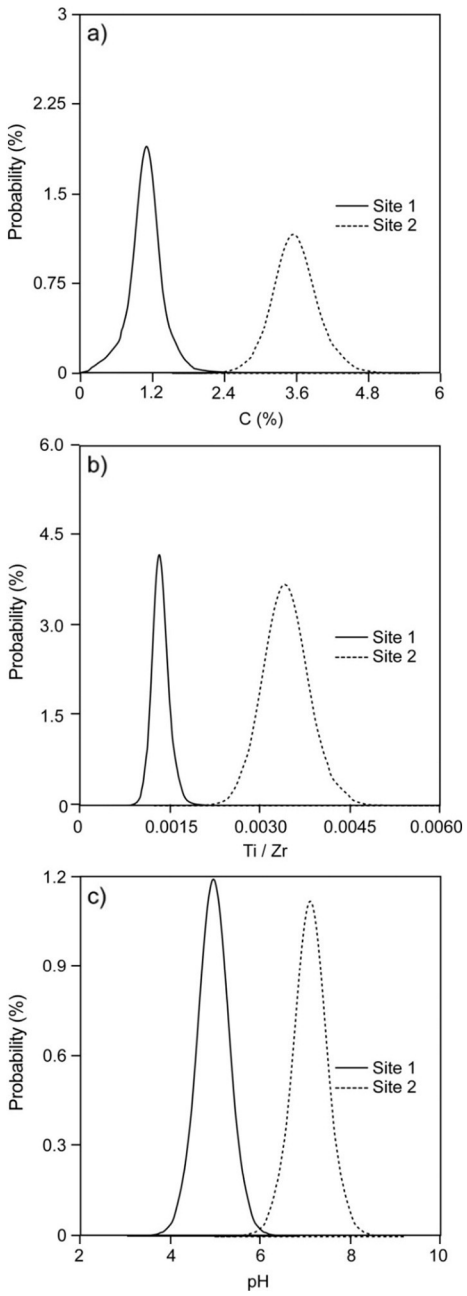

Fig. 4. Posterior marginal distributions of various soil properties predicted at two selected locations (marked in Fig. 3) and including; a) total soil carbon (C – %), b) Ti/Zr ratio, c) pH, respectively.

3.7. Spatial distribution of predicted soil properties using INLA-SPDE

Fig. 5 shows the spatial distributions of the mean and credible interval of predicted soil properties due to the uncertainty of the model parameters only across the study area. Here, the credible interval was delineated by the differences between 5% and 95% percentiles of the predicted soil properties. In terms of the strongly skewed C, an increasing trend was identified from west to east across the study area (Fig. 5a). This was mostly driven by elevation, soil types and land use (Li et al., 2015a, 2015b; Shi et al., 2015; Stockmann et al., 2016). In the east of the study area dominated by Vertisols and native vegetation, the elevation was high, so was the soil C. Conversely, lower C values were found in the western plains with Luvisols and Solonetz whereby the land was mostly used for cropping.

The large uncertainty (~2%) was located at the eastern corner of the study area (Fig. 5b). This was consistent with the posterior marginal distribution of the predicted soil C (Fig. 4a). Again, it was most likely because the INLA-SPDE model failed to accurately estimate the soil C values in these due to the short-scale variation in the covariates (i.e. elevation and TWI). In addition, large uncertainty was found along several strips across the study area. This was particularly the case in a southeast to northwest trending band in the western third of the study area. The uncertainty was probably caused by the large TWI values, corresponding to a small wooded depression (see Fig. 1).

Fig. 5c and d show the spatial distributions of the mean and credible interval of predicted Ti/Zr ratio. The pattern was similar to that found for soil C, whereby Ti/Zr ratio increased from west to east. Similarly, this was mainly driven by soil types, parent materials and land use (Stockmann et al., 2016). Unlike soil C, the largest model uncertainty for predicting Ti/Zr ratio was only identified at the eastern margins of the study area. Again this was most likely due to the poor performance of the INLA-SPDE model as a function of the highly variable nature of the covariates.

However, this was not the case for pH. As shown in Fig. 5e, soil pH increased from quite acidic (~5) in the southwest to moderately to strongly alkaline (~8.5) in the northeast. As was shown in Fig. 5f, the largest credibility interval of the predicted pH was mostly located close to the margins. In this case, the large credibility interval values were mainly due to the edge effect.

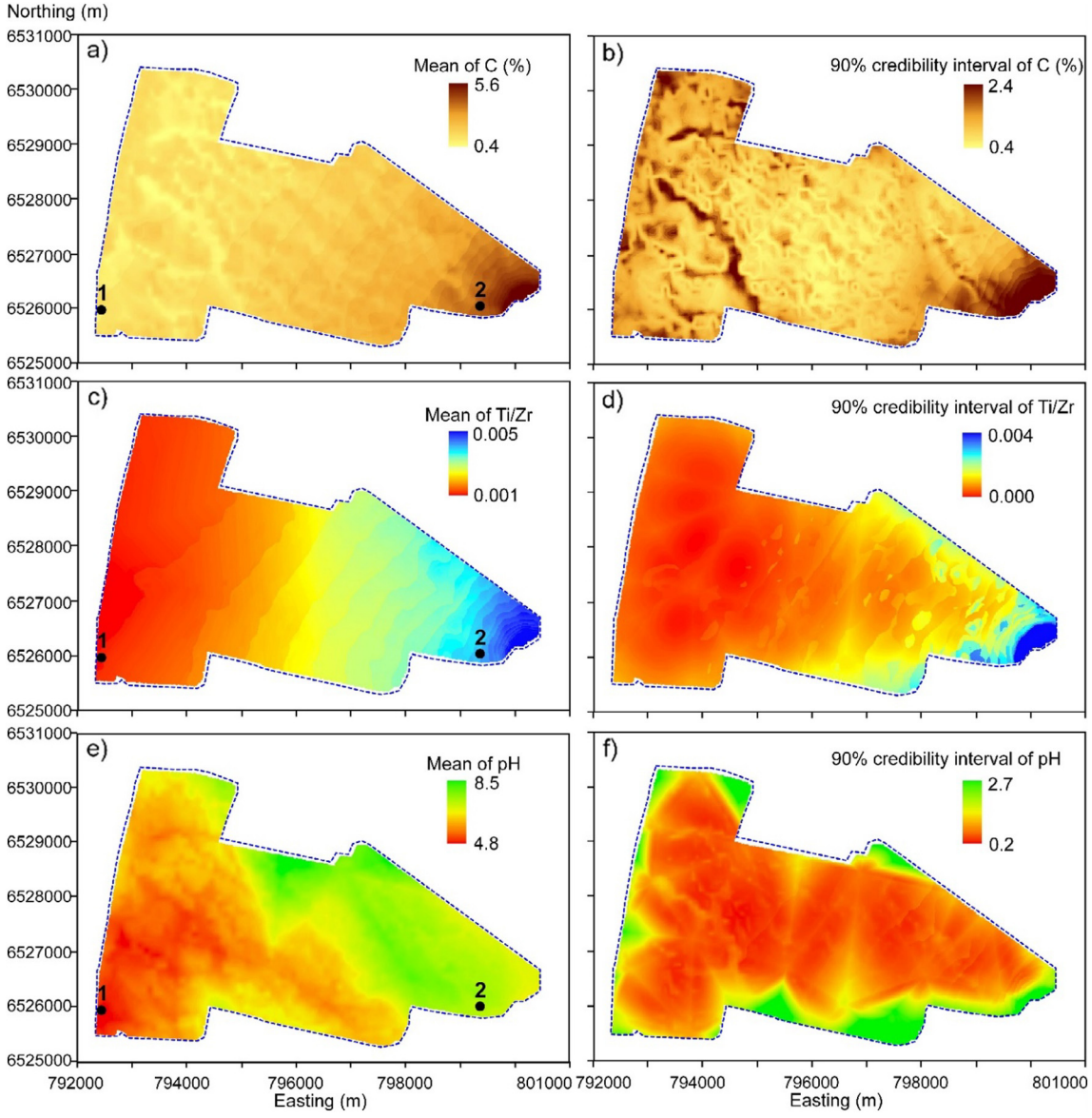

Fig. 5. Spatial distributions of the predicted soil properties using INLA-SPDE and including; a) total soil carbon (C – %), c) Ti/Zr ratio, e) pH; and spatial distributions of the 90% credibility interval for soil b) C, d) Ti/Zr ratio and f) pH, respectively. Note: two selected sites with predicted small and large soil properties were marked with black dots.

3.8. Spatial distribution of predicted soil properties using REML-LMM

For comparison, the spatial distributions of the mean and prediction interval of predicted soil properties generated by REML-LMM were presented (Fig. 6). Here, the prediction interval was delineated by the differences between 5% and 95% percentiles of the predicted soil properties and was calculated using the mean and kriging variance of the *E*-BLUP assuming a Gaussian distribution.

In terms of predicting soil C, REML-LMM produced similar mean values compared with INLA-SPDE (Fig. 6a). However, this was not the case for the prediction interval (Fig. 6b). Although the spatial pattern of the model uncertainty was similar, REML-LMM had a much larger 90% prediction interval (3.2–3.8%) compared with INLA-SPDE (0.4–2.4%). This was not unexpected given the differences in the two methods. Specifically, REML-LMM represents the prediction interval, while INLA-SPDE only shows credible (or confidence interval in frequentist statistic).

With regard to Ti/Zr ratio (Fig. 6c), REML-LMM was found to produce lower Ti/Zr ratio (~0.001) at the western part and higher Ti/Zr ratio (0.005) at the eastern corner of the study area compared with INLA-SPDE. As for soil pH, the mean of the prediction achieved by REML-LMM was similar to that of INLA-SPDE (Fig. 6e).

3.9. Implications for environmental monitoring and management

The characteristics of INLA-SPDE demonstrated here may be applied in a number of ways. Firstly, given the capability of estimating the posterior distributions of the model parameters and responses, it is possible to use INLA-SPDE as an alternative method to the traditional computationally intensive MCMC-based approach (Banerjee et al., 2008; Orton et al., 2009; Minasny et al., 2011).

Secondly, the ease of incorporating various likelihood functions (e.g. Gaussian, log-normal) of INLA-SPDE makes it suitable for predicting various environmental properties and estimating the posterior marginal distributions of the predicted values. Unlike the traditional or model-based geostatistics which relied on data transformation (Orton et al., 2009) or Copulas (Marchant et al., 2011), INLA-SPDE is also able to deal with the skewed data with the latent Gaussian field directly in the model and is proven to be as robust as REML-LMM (in this study) and Generalized Additive Models with Gaussian simulations (Poggio

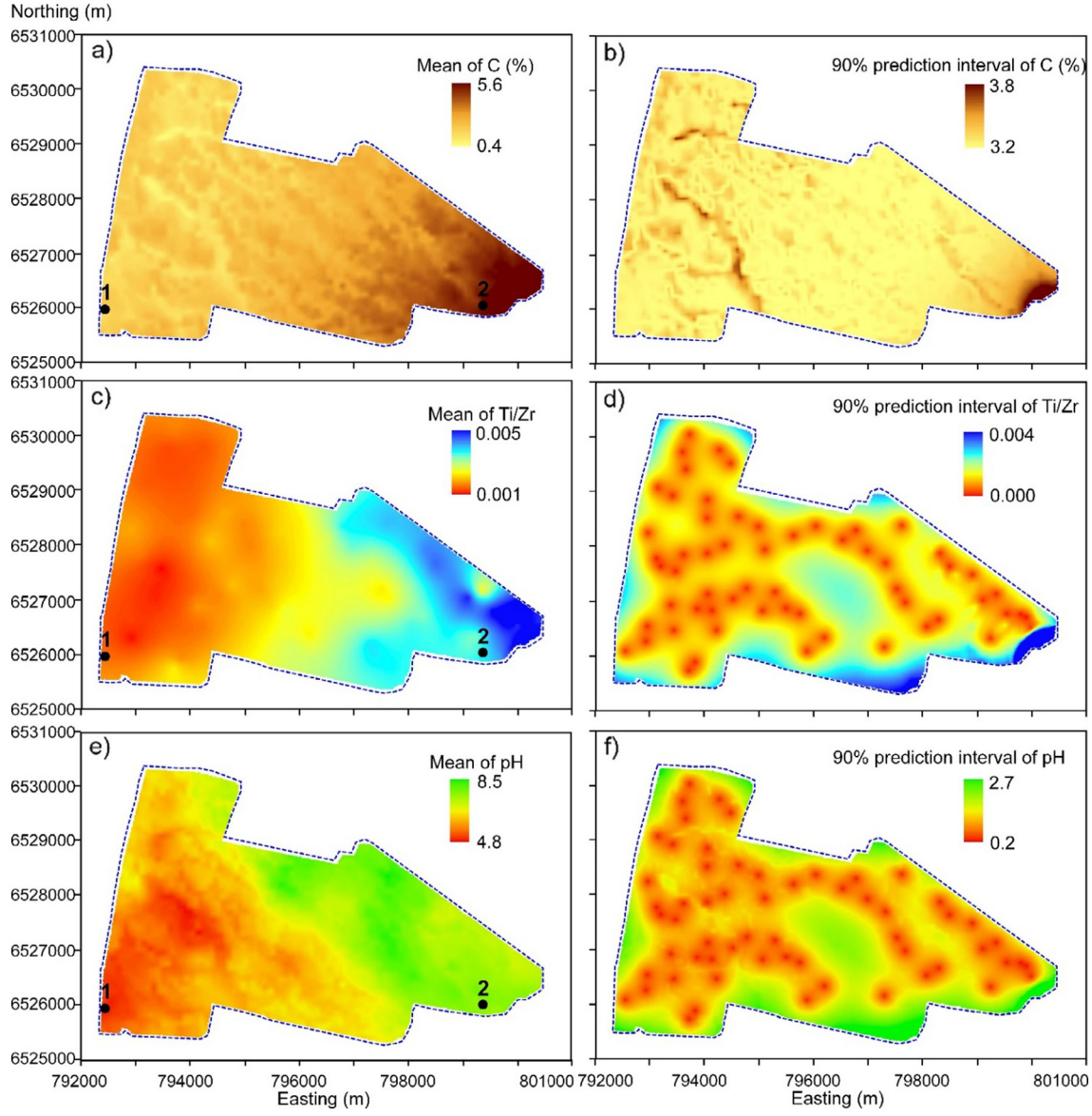

Fig. 6. Spatial distributions of the predicted soil properties using REML-LMM and including; a) total soil carbon (C – %), c) Ti/Zr ratio, e) pH; and spatial distributions of the 90% prediction intervals for soil b) C, d) Ti/Zr ratio and f) pH, respectively. Note: two selected sites with predicted small and large soil properties were marked with black dots.

et al., 2016). Therefore, INLA-SPDE can be potentially applied in mapping the spatial distribution of various environmental variables and pollutions (Teng et al., 2014; Yang et al., 2014; Liu et al., 2016; Gómez-Nubla et al., 2017) and establishing risk management zones with using the posterior marginal distributions of the prediction (Horta et al., 2015; Beaudequin et al., 2016; O'Rourke et al., 2016).

Thirdly, it is also worth highlighting the robustness of INLA-SPDE with small calibration datasets. As suggested by Webster and Oliver (1992), ~100 samples are often required for accurately estimating a variogram. However, as demonstrated in our study, 40–60 samples were sufficient to establish a "good" INLA-SPDE model for predicting strongly skewed and non-skewed soil properties provided that strongly correlated ancillary data were available (Stockmann et al., 2016). This suggests that INLA-SPDE could be employed when a detailed sampling campaign is not available.

Lastly, it should be noted that while REML-LMM can only estimate the parameter uncertainty based on an approximation of the Fisher information matrix assuming Gaussian distribution (Minasny and McBratney, 2005), INLA-SPDE is able to calculate the posterior distribution of parameters. This information can be used to assist decision-making in environmental management (Yang et al., 2016). However, to calculate the prediction interval equivalent to kriging variance, simulations of the model parameters need to be done.

3.10. Disadvantages of INLA-SPDE

A number of disadvantages of INLA-SPDE were also reported in the study. First, some discontinuous artefacts were identified in the maps of predicted soil C (Fig. 5a) and Ti/Zr ratio (Fig. 5c). This was most likely due to the triangulated meshes, which were used to approximate the SPDE functions (Simpson et al., 2012).

Second, it should be also noted that the INLA-SPDE approach took ~24 h to calculate the credible intervals of each of the soil properties (particularly for non-Gaussian distributed variables) across the 10-m grid using a computer with an Intel (R) Core (TM) i7-4510U CPU @ 2.00GHz and a RAM of 8.00 GB. Unlike INLA-SPDE, the time of estimating the optimal model parameters was much shorter (i.e. ~1 min) for REML-LMM although REML-LMM was not able to estimate the posterior marginal distribution of the model parameters. It was also reported by Poggio et al. (2016) that INLA-SPDE became quite slow when estimating the posterior marginal distributions of the environmental variables associated with large datasets using non-Gaussian likelihood families.

4. Conclusions

The spatial distribution of various skewed and non-skewed environmental variables (e.g. soil Carbon, pH, and elemental Fe, Ca, K, and Ti/Zr) were predicted using a Bayesian inference approach, Integrated Nested Laplace Approximation with Stochastic Partial Differential Equation (INLA-SPDE). Based on independent validation datasets, it was found that INLA-SPDE was equivalent to a linear mixed model estimated by residual maximum likelihood (REML-LMM) in terms of the model performance and was similarly robust with sparse datasets.

The advantage of INLA-SPDE was that it was able to predict the posterior marginal distributions of the model parameters as well as the model responses without carrying out extensive simulations. Therefore, INLA-SPDE can be potentially applied in mapping the spatial distribution of environmental variables via various likelihood families and estimating their posterior marginal distributions to assist decision making in environmental management. However, the use of triangulated meshes in INLA-SPDE may lead to discontinuous artefacts of the model responses and the computation time will become quite long when dealing with non-Gaussian likelihood families.

References

Banerjee, S., Gelfand, A.E., Finley, A.O., Sang, H., 2008. Gaussian predictive process models for large spatial data sets. J. R. Stat. Soc. Ser. B Stat Methodol. 70, 825–848.

Beaudequin, D., Harden, F., Roiko, A., Mengersen, K., 2016. Utility of Bayesian networks in QMRA-based evaluation of risk reduction options for recycled water. Sci. Total Environ. 541, 1393–1409.

Bishop, T.F.A., Minasny, B., McBratney, A.B., 2006. Uncertainty analysis for soil-terrain models. Int. J. Geogr. Inf. Sci. 20, 117–134.

Blangiardo, M., Cameletti, M., Baio, G., Rue, H., 2013. Spatial and spatio-temporal models with R-INLA. Spat. Spatiotemporal Epidemiol. 7, 39–55.

BOM (Bureau of Meteorology), 2016. Climate Averages for Gunnedah SCS. http://www.bom.gov.au/climate/averages/tables//cw_055024.shtml.

Brus, D.J., Bogaert, P., Heuvelink, G.B.M., 2008. Bayesian maximum entropy prediction of soil categories using a traditional soil map as soft information. Eur. J. Soil Sci. 59, 166–177.

Chen, L., Shen, Z., Yang, X., Liao, Q., Shaw, L.Y., 2014. An interval-deviation approach for hydrology and water quality model evaluation within an uncertainty framework. J. Hydrol. 509, 207–214.

Conrad, O., Bechtel, B., Bock, M., Dietrich, H., Fischer, E., Gerlitz, L., Wehberg, J., Wichmann, V., Böhner, J., 2015. System for automated geoscientific analyses (SAGA) v. 2.1.4. Geosci. Model Dev. 8, 1991–2007.

Core Team, R., 2017. R: a Language and Environment for Statistical Computing. R Foundation for Statistical Computing, Vienna.

De Gruijter, J.J., Minasny, B., Mcbratney, A.B., 2015. Optimizing stratification and allocation for design-based estimation of spatial means using predictions with error. J. Surv. Stat. Methodol. 3, 19–42.

De Gruijter, J.J., McBratney, A.B., Minasny, B., Wheeler, I., Malone, B.P., Stockmann, U., 2016. Farm-scale soil carbon auditing. Geoderma 265, 120–130.

Dierke, C., Werban, U., 2013. Relationships between gamma-ray data and soil properties at an agricultural test site. Geoderma 199, 90–98.

Diggle, P.J., Tawn, J.A., Moyeed, R.A., 1998. Model-based geostatistics. J. R. Stat. Soc. Ser. C Appl. Stat. 47, 299–326.

D'Or, D., Bogaert, P., 2003. Continuous-valued map reconstruction with the Bayesian maximum entropy. Geoderma 112, 169–178.

Douaik, A., Van Meirvenne, M., Tóth, T., 2005. Soil salinity mapping using spatio-temporal kriging and Bayesian maximum entropy with interval soft data. Geoderma 128, 234–248.

Eidsvik, J., Finley, A.O., Banerjee, S., Rue, H., 2012. Approximate Bayesian inference for large spatial datasets using predictive process models. Comput. Stat. Data An. 56, 1362–1380.

Gelman, A., Carlin, J.B., Stren, H.S., Rubin, D.B., 2004. Bayesian Data Analysis. Chapman & Hall, Boca Raton, Florida, USA.

Gómez-Nubla, L., Aramendia, J., de Vallejuelo, S.F.O., Madariaga, J.M., 2017. Contamination study of forest track soils located in a recreational area and filled with steel industry waste 30 years ago. Sci. Total Environ. 598, 28–37.

Guimaraes, S.N.P., Hamza, V.M., da Silva, J.J., 2013. Airborne geophysical surveys in the north-central region of Goias (Brazil): implications for radiometric characterization of tropical soils. J. Environ. Radioact. 116, 10–18.

Haskard, K.A., Rawlins, B.G., Lark, R.M., 2010. A linear mixed model, with non-stationary mean and covariance, for soil potassium based on gamma radiometry. Biogeosciences 7, 2081–2089.

Heuvelink, G.B., Burrough, P.A., Stein, A., 2006. Developments in analysis of spatial uncertainty since 1989. In: Fisher, P., et al. (Eds.), Classics from IJGIS; twenty years of the International Journal of Geographical Information Science and Systems. Taylor & Francis, pp. 91–95.

Horta, A., Malone, B., Stockmann, U., Minasny, B., Bishop, T.F.A., McBratney, A.B., Pallasser, R., Pozza, L., 2015. Potential of integrated field spectroscopy and spatial analysis for enhanced assessment of soil contamination: a prospective review. Geoderma 241, 180–209.

Huang, J., Zare, E., Malik, R.S., Triantafilis, J., 2015. An error budget for soil salinity mapping using different ancillary data. Soil Res. 53, 561–575.

Huang, J., Minasny, B., Whelan, B.M., McBratney, A.B., Triantafilis, J., 2017a. Temperature-dependent hysteresis effects on EM induction instruments: an example of single-frequency multi-coil array instruments. Comput. Electron. Agric. 132, 76–85.

Huang, J., Pedrera-Parrilla, A., Vanderlinden, K., Taguas, E.V., Gómez, J.A., Triantafilis, J., 2017b. Potential to map depth-specific soil organic matter content across an olive grove using quasi-2d and quasi-3d inversion of DUALEM-21 data. Catena 152, 207–217.

Kavetski, D., Kuczera, G., Franks, S.W., 2006. Bayesian analysis of input uncertainty in hydrological modeling: 2. Application. Water Resour. Res. 42 (3).

Krainski, E.T., Lindgren, F., Simpson, D., Rue, H., 2016. The R-INLA Tutorial on SPDE Models. Available from. https://www.math.ntnu.no/inla/r-inla.org/tutorials/spde/spde-tutorial.pdf.

Lark, R.M., Cullis, B.R., 2004. Model-based analysis using REML for inference from systematically sampled data on soil. Eur. J. Soil Sci. 55, 799–813.

Lark, R.M., Cullis, B.R., Welham, S.J., 2006. On spatial prediction of soil properties in the presence of a spatial trend: the empirical best linear unbiased predictor (E-BLUP) with REML. Eur. J. Soil Sci. 57, 787–799.

Li, S., Shi, Z., Chen, S., Ji, W., Zhou, L., Yu, W., Webster, R., 2015a. In situ measurements of organic carbon in soil profiles using vis-NIR spectroscopy on the Qinghai–Tibet plateau. Environ. Sci. Technol. 49, 4980–4987.

Li, H.Y., Webster, R., Shi, Z., 2015b. Mapping soil salinity in the Yangtze delta: REML and universal kriging (E-BLUP) revisited. Geoderma 237, 71–77.

Liang, S., Jia, H., Xu, C., Xu, T., Melching, C., 2016. A Bayesian approach for evaluation of the effect of water quality model parameter uncertainty on TMDLs: a case study of Miyun reservoir. Sci. Total Environ. 560, 44–54.

Lin, L.I.K., 1989. A concordance correlation coefficient to evaluate reproducibility. Biometrics 255–268.

Lindgren, F., 2012. Continuous domain spatial models in r-inla. ISBA Bull. 19, 14–20.

Lindgren, F., Rue, H., 2015. Bayesian spatial modelling with R-INLA. J. Stat. Softw. 63.
Lindgren, F., Rue, H., Lindström, J., 2011. An explicit link between Gaussian fields and Gaussian Markov random fields: the stochastic partial differential equation approach. J. R. Stat. Soc. Ser. B Stat Methodol. 73, 423–498.
Liu, S., McGree, J., Hayes, J.F., Goonetilleke, A., 2016. Spatial response surface modelling in the presence of data paucity for the evaluation of potential human health risk due to the contamination of potable water resources. Sci. Total Environ. 566, 1368–1378.
Marchant, B.P., Saby, N.P.A., Jolivet, C.C., Arrouays, D., Lark, R.M., 2011. Spatial prediction of soil properties with copulas. Geoderma 162, 327–334.
Martins, I.F., Teixeira, A.L., Pinheiro, L., Falcao, A.O., 2012. A Bayesian approach to in silico blood-brain barrier penetration modeling. J. Chem. Inf. Model. 52, 1686–1697.
McBratney, A.B., 1992. On variation, uncertainty and informatics in environmental soil management. Soil Res. 30, 913–935.
Milledge, D.G., Lane, S.N., Heathwaite, A.L., Reaney, S.M., 2012. A Monte Carlo approach to the inverse problem of diffuse pollution risk in agricultural catchments. Sci. Total Environ. 433, 434–449.
Minasny, B., McBratney, A.B., 2005. The Matérn function as a general model for soil variograms. Geoderma 128, 192–207.
Minasny, B., McBratney, A.B., 2007. Spatial prediction of soil properties using EBLUP with the Matérn covariance function. Geoderma 140, 324–336.
Minasny, B., McBratney, A.B., 2016. Digital soil mapping: a brief history and some lessons. Geoderma 264, 301–311.
Minasny, B., McBratney, A.B., Lark, R.M., 2008. Digital soil mapping technologies for countries with sparse data infrastructures. Digital Soil Mapping with Limited Data. Springer Netherlands, pp. 15–30.
Minasny, B., Vrugt, J.A., McBratney, A.B., 2011. Confronting uncertainty in model-based geostatistics using Markov Chain Monte Carlo simulation. Geoderma 163, 150–162.
Musenge, E., Chirwa, T.F., Kahn, K., Vounatsou, P., 2013. Bayesian analysis of zero inflated spatiotemporal HIV/TB child mortality data through the INLA and SPDE approaches: applied to data observed between 1992 and 2010 in rural North East South Africa. Int. J. Appl. Earth Obs. Geoinf. 22, 86–98.
Nelson, M.A., Bishop, T.F.A., Triantafilis, J., Odeh, I.O.A., 2011. An error budget for different sources of error in digital soil mapping. Eur. J. Soil Sci. 62, 417–430.
O'Rourke, S.M., Stockmann, U., Holden, N.M., McBratney, A.B., Minasny, B., 2016. An assessment of model averaging to improve predictive power of portable vis-NIR and XRF for the determination of agronomic soil properties. Geoderma 279, 31–44.
Orton, T.G., Rawlins, B.G., Lark, R.M., 2009. Using measurements close to a detection limit in a geostatistical case study to predict selenium concentration in topsoil. Geoderma 152, 269–282.
Pebesma, E.J., 2004. Multivariable geostatistics in S: the gstat package. Comput. Geosci. 30, 683–691.
Poggio, L., Gimona, A., Spezia, L., Brewer, M.J., 2016. Bayesian spatial modelling of soil properties and their uncertainty: the example of soil organic matter in Scotland using R-INLA. Geoderma 277, 69–82.
Ribeiro Jr., P.J., Diggle, P.J., 2001. geoR: a package for geostatistical analysis. R-News 1, 14–18.
Rong, Q., Cai, Y., Chen, B., Yue, W., Yin, X.A., Tan, Q., 2017. An enhanced export coefficient based optimization model for supporting agricultural nonpoint source pollution mitigation under uncertainty. Sci. Total Environ. 580, 1351–1362.
Rue, H., Martino, S., Chopin, N., 2009. Approximate Bayesian inference for latent Gaussian models by using integrated nested Laplace approximations. J. R. Stat. Soc. Ser. B Stat Methodol. 71, 319–392.
Rue, H., Riebler, A., Sørbye, S.H., Illian, J.B., Simpson, D.P., Lindgren, F.K., 2016. Bayesian Computing with INLA: A Review. arXiv preprint arXiv:1604.00860.
Ryan, E.G., Drovandi, C.C., McGree, J.M., Pettitt, A.N., 2016. A review of modern computational algorithms for Bayesian optimal design. Int. Stat. Rev. 1, 128–154.
Schrödle, B., Held, L., 2011. Spatio-temporal disease mapping using INLA. Environmetrics 22, 725–734.
Schuler, U., Erbe, P., Zarei, M., Rangubpit, W., Surinkum, A., Stahr, K., Herrmann, L., 2011. A gamma-ray spectrometry approach to field separation of illuviation-type WRB reference soil groups in northern Thailand. J. Plant Nutr. Soil Sci. 174, 536–544.
Shi, Z., Ji, W., Viscarra Rossel, R.A., Chen, S., Zhou, Y., 2015. Prediction of soil organic matter using a spatially constrained local partial least squares regression and the Chinese vis–NIR spectral library. Eur. J. Soil Sci. 66, 679–687.
Simpson, D., Lindgren, F., Rue, H., 2012. Think continuous: Markovian Gaussian models in spatial statistics. Spat. Stat. 1, 16–29.
Stockmann, U., Cattle, S.R., Minasny, B., McBratney, A.B., 2016. Utilizing portable X-ray fluorescence spectrometry for in-field investigation of pedogenesis. Catena 139, 220–231.
Sudduth, K.A., Drummond, S.T., Kitchen, N.R., 2001. Accuracy issues in electromagnetic induction sensing of soil electrical conductivity for precision agriculture. Comput. Electron. Agric. 31, 239–264.
Teng, H., Shi, Z., Ma, Z., Li, Y., 2014. Estimating spatially downscaled rainfall by regression kriging using TRMM precipitation and elevation in Zhejiang Province, southeast China. Int. J. Remote Sens. 35, 7775–7794.
Tierney, L., Kadane, J.B., 1986. Accurate approximations for posterior moments and marginal densities. J. Am. Stat. Assoc. 81, 82–86.
Triantafilis, J., Gibbs, I., Earl, N., 2013. Digital soil pattern recognition in the lower Namoi valley using numerical clustering of gamma-ray spectrometry data. Geoderma 192, 407–421.
Viscarra Rossel, R.A., McBratney, A.B., 1998. Soil chemical analytical accuracy and costs: implications from precision agriculture. Anim. Prod. Sci. 38, 765–775.
Viscarra Rossel, R.A., Taylor, H.J., McBratney, A.B., 2007. Multivariate calibration of hyperspectral γ-ray energy spectra for proximal soil sensing. Eur. J. Soil Sci. 58, 343–353.
Webster, R., Oliver, M.A., 1992. Sample adequately to estimate variograms of soil properties. J. Soil Sci. 43, 177–192.
Wilford, J.R., Bierwirth, P.N., Craig, M.A., 1997. Application of airborne gamma-ray spectrometry in soil/regolith mapping and applied geomorphology. AGSO J. Aust. Geol. Geophys. 17, 201–216.
Wong, M.T.F., Harper, R.J., 1999. Use of on-ground gamma-ray spectrometry to measure plant-available potassium and other topsoil attributes. Aust. J. Soil Res. 37, 267–277.
Wong, M.T.F., Asseng, S., Robertson, M.J., Oliver, Y., 2008. Mapping subsoil acidity and shallow soil across a field with information from yield maps, geophysical sensing and the grower. Precis. Agric. 9, 3–15.
Yang, X.H., She, D.X., Yang, Z.F., Tang, Q.H., Li, J.Q., 2009. Chaotic Bayesian method based on multiple criteria decision making (MCDM) for forecasting nonlinear hydrological time series. Int. J. Nonlinear Sci. Numer. Simul. 10, 1595–1610.
Yang, X., Mei, Y., He, J., Jiang, R., Li, Y., Li, J., 2014. Comprehensive assessment for removing multiple pollutants by plants in bioretention systems. Chin. Sci. Bull. 59, 1446–1453.
Yang, X.H., Sun, B.Y., Zhang, J., Li, M.S., He, J., Wei, Y.M., Li, Y.Q., 2016. Hierarchy evaluation of water resources vulnerability under climate change in Beijing. Chin. Nat. Haz. 84, 63–76.
Zhou, B., Zhang, X.G., Wang, R.C., 2004. Automated soil resources mapping based on decision tree and Bayesian predictive modeling. J. Zhejiang Univ. (Sci.) 5, 782–795.